SO_2 promoted in situ recovery of thermally deactivated $Fe_2(SO_4)_3/TiO_2$ NH_3- ᴛ SCR catalysts: From experimental work to theoretical study

Yanke Yu[a], Changwei Chen[a], Mudi Ma[a], Mark Douthwaite[b], Chi He[a,b,], Jifa Miao[c], Jinsheng Chen[c,], Can Li[d]

[a] Department of Environmental Science and Engineering, School of Energy and Power Engineering, Xi'an Jiaotong University, Xi'an 710049, PR China
[b] Cardiff Catalysis Institute, School of Chemistry, Cardiff University, Main Building, Park Place, Cardiff CF10 3AT, UK
[c] Center for Excellence in Regional Atmospheric Environment, Institute of Urban Environment, Chinese Academy of Sciences, Xiamen 361021, PR China
[d] Center for Coordination Bond Engineering, College of Materials Science and Engineering, China Jiliang University, Hangzhou 310018, PR China

HIGHLIGHTS

- Thermally deactivated $Fe_2(SO_4)_3/TiO_2$ (FeTi-T) was obtained by thermal treatment.
- $Fe_2(SO_4)_3$ decomposition causes Brønsted acid sites loss and catalyst deactivation.
- The in situ recovery of FeTi-T is achieved by SO_2 in the flue gas.
- $Fe_2(SO_4)_3$ is formed by SO_2/O_2 and Fe_2O_3 under NH_3-SCR reaction conditions.

GRAPHICAL ABSTRACT

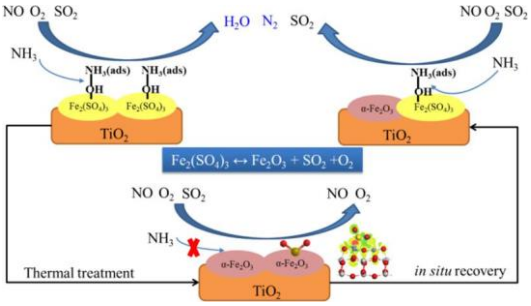

ARTICLE INFO

Keywords:
NH_3-SCR
Fe2(SO4)3
Thermal deactivation
In situ recovery
DFT calculations

ABSTRACT

Due to high catalytic activity and excellent resistance to SO_2 and H_2O, sulfate materials are considered to be promising vanadium-free catalysts for selective catalytic reduction of NO_x with NH_3 (NH_3-SCR). Despite this, investigations about thermal stability of sulfate SCR catalysts are limited, which is surprising given that sulfates are typically susceptible to thermal decomposition. In this work, the thermal stability of $Fe_2(SO_4)_3/TiO_2$ catalysts was investigated. It was determined that the thermal decomposition of $Fe_2(SO_4)_3$ resulted in NO_x conversion decreased from 90% to 60% at 350 °C. Interestingly however, the introduction of SO_2 into the gas stream was found to reverse the effects of the thermal deactivation and the NO_x conversion of 90% (350 °C) was once again observed. Extensive characterization of each catalyst sample and density functional theory (DFT) calculations were subsequently conducted. The reduction in catalytic activity after the thermal treatment was attributed to the transformation of $Fe_2(SO_4)_3$ to α-Fe_2O_3, which reduced the quantity of Brønsted acid sites on the catalyst. The presence of SO_2 in the gas stream was found to reverse this phase transformation which ultimately led to the recovery of Brønsted acid sites. DFT calculations indicated that SO_2 adsorbed selectively on Fe atoms of the thermal deactivated catalysts and S-Fe bond should mainly be formed by electrons from p orbitals of S and Fe atoms. Then NH_3 could be adsorbed on the surface by N-S bond with SO_2. The recoverable property of this catalyst provides a promising outlook for the commercial application, especially given that industrial flue gas streams regularly contain SO_2.

Corresponding authors at: Department of Environmental Science and Engineering, School of Energy and Power Engineering, Xi'an Jiaotong University, Xi'an 710049, PR China (C. He).
E-mail addresses: chi_he@xjtu.edu.cn (C. He), jschen@iue.ac.cn (J. Chen).

1. Introduction

The selective catalytic reduction of NO_x with NH_3 (NH_3-SCR) is an effective approach to controlling the emission of NO_x from the com-bustion of fossil fuels [1–4]. This approach has also been shown to be highly successful for NO_x abatement in the exhausts of diesel engines [5–7]. Current commercial SCR catalysts are typically vanadium-based materials which are due to their high efficiency for NO_x removal and excellent tolerance of SO_2. Nevertheless, it is vitally important that novel vanadium-free SCR catalysts are developed because of the bio-logical toxicity of vanadium-based catalysts and their undesirable ac-tivity for SO_2 oxidation [8–10]. There are numerous examples of transition metal (e.g., Mn, Ce, Fe, and Cu) oxide catalysts which are highly active for NH_3-SCR [11–14]. However, in many cases these catalysts are exceptionally susceptible to deactivation in the presence of SO_2 (a common component in flue gas), which has greatly limited the application of these vanadium-free catalysts [15–18]. The deactivation of these vanadium-free catalysts is believed to be a result of interactions between SO_2/O_2 and active sites, which leads to changes in the surface acidity and reducibility and ultimately results in the deactivation of these catalytic materials [15–18]. Various sulfate catalysts have also been investigated for their application in NH_3-SCR [19,20]. Interest-ingly, it was revealed that some of these sulfate catalysts possessed an abundance of acid sites and displayed reasonable SCR activity and SO_2 resistance. $Fe_2(SO_4)_3/TiO_2$ catalysts for instance were found to be highly active as NO_x conversion up to 90% were observed at reaction temperatures in excess of 350 °C [19]. Even higher NO_x conversions were observed over a $CuSO_4/TiO_2$ catalyst (> 90%) in temperatures ranging from 280 to 380 °C [20]. In addition, both of these sulfate catalysts displayed excellent resistances to SO_2, underlining their po-tential as catalysts for industrial NO_x reduction [19,20].

The thermal stability of catalysts is an important property to in-vestigate when assessing the commercial viability of a catalyst for NH_3-SCR [21,22]. In commercial flue gas streams, large fluctuations in temperature are common and temperatures in excess of 600 °C can be observed under certain conditions [22]. At such elevated temperatures, the destruction of the framework/pore structure of oxide-based mate-rials has been shown to occur which is considered to be another me-chanism commonly associated with catalytic deactivation [23,24]. Ty-pically, sulfates are prone to decomposition at high temperatures (e.g., the initial decomposition of $Fe_2(SO_4)_3$ and $CuSO_4$ in flowing air was 507 and 586 °C, respectively [25]), which may also lead to the thermal deactivation of sulfate catalysts. As such, the poor thermal stability of these sulfate catalysts may hinder their practical application in NH_3-SCR systems. However, few researchers have highlighted the issues associated with the thermal deactivation of these materials in NH_3-SCR.

The promotional effect of SO_2 on some vanadium-free oxide cata-lysts at given temperatures have been reported [26–29]. L. Ma et al. [28] studied the influence of SO_2 sulfation treatment on CeO_2 cubes and nanospheres and they found the treatment could significantly increase the SCR activity of the catalyst at temperatures higher than 200 °C due to the formation of surface $Ce_2(SO_4)_3$, which could supply abundant Brønsted acid sites. F. Liu et al. [29] found that SO_2 treatment could lead to the formation of the sulfate species with iron sites, resulting in the enhancement of acid strength on $FeTiO_x$ catalysts, thus increased the SCR activity at temperatures higher than 325 °C. As such, it is ra-tional to postulate that the presence of SO_2 in flue gas may assist in the regeneration of sulfate species on the surface of sulfate catalysts which have undergone thermal deactivation in NH_3-SCR. If this theory is correct, the in situ recovery may be achieved and thermally-deactivated sulfate catalysts may not have to be replaced. This would be highly advantageous both practically and economically from an industrial perspective and as such, would provide a novel approach for the future catalyst design of SCR catalysts.

Density functional theory (DFT) is thought to be an efficient method in the study of catalysts deactivation and regeneration [30,31]. In this work, both experimental methods and DFT calculations were employed to investigate the thermal deactivation and regeneration of $Fe_2(SO_4)_3/TiO_2$ SCR catalysts. $Fe_2(SO_4)_3$ was selected preferentially over $CuSO_4$ due to its lower thermal stability [25]. In order to investigate the effect of thermal stability on the performance of this catalyst for NO_x con-version, the prepared catalyst was calcined under a flow of N_2 at 630 °C for 1 h. The recovery in the catalytic activity of the thermally-deacti-vated catalyst was assessed in the presence of SO_2 at 350 °C. N_2 ad-sorption–desorption, X-Ray diffraction (XRD), Thermogravimetric analysis (TGA), Fourier-transform infrared spectroscopy (FTIR), X-ray photoelectron spectroscopy (XPS), Temperature-programmed deso-rption of NH_3 (NH_3-TPD), Temperature-programmed reduction of H_2 (H_2-TPR) and in situ diffuse reflectance infrared Fourier transform spectroscopy (in situ DRIFTS) were used to investigate the mechanism of thermal deactivation and recovery of catalytic activity. DFT calcula-tions were performed to investigate the adsorption of SO_2 on the thermal deactivated catalysts and the influence of SO_2 on NH_3 ad-sorption.

2. Experimental section

2.1. Catalyst preparation

$Fe_2(SO_4)_3/TiO_2$ catalyst was synthetized by a solid-state impregna-tion method. Firstly, a sol-gel method was used to obtain anatase TiO_2 support material [20]. Subsequently, $Fe_2(SO_4)_3$ (0.6 g) was added to the synthesized TiO_2 (6.0 g) in an agate mortar and ground to uniformity. The powdered mixture was then calcined at 500 °C in air for 5 h to yield the fresh $Fe_2(SO_4)_3/TiO_2$ catalyst (FeTi). A thermal treatment of this material was subsequently performed in a tubular furnace. For this, the fresh $Fe_2(SO_4)_3/TiO_2$ catalyst was calcined under N_2 flow at 630 °C for 1 h to yield the thermally deactivated catalyst (FeTi-T).

2.2. NO_x conversion tests

The NO_x conversion of each catalyst material was tested using a fixed-bed quartz reactor (φ 10 mm × 600 mm). The gas mixture con-tained NO (600 ppm), NH_3 (600 ppm), H_2O (4.0%) and O_2 (4.0%) in N_2. The total gas flow rate was maintained at 1200 mL/min, which corre-sponded to a gas hourly space velocity (GHSV) of 60 000 h^{-1}. Concentrations of NO and NO_2 in the gas were detected using a T-340 flue gas analyzer (Testo Company, Germany). A SENMA IR Sensor (Madur Company, Austria) was used to analyze the concentration of N_2O in the outlet. NO_x conversion was calculated by Eq. (1):

$$x = \frac{NO_{x,in} - NO_{x,out}}{NO_{x,in}} \times 100\% \quad (1)$$

where $NO_{x,in}$ and $NO_{x,out}$ were concentrations of NO_x (NO + NO_2) in the inlet and outlet of the reactor, respectively.

N_2O is the main by-product of SCR reaction and the N_2 selectivity was calculated by Eq. (2):

$$S_{N_2} = 1 - \frac{2N_2O_{out}}{NO_{x,in} - NO_{x,out}} \times 100\% \quad (2)$$

where N_2O_{out} was the concentrations of N_2O in the outlet of the reactor.

2.3. Activity recovery of the thermally-deactivated catalyst

A similar experimental set up was also used to investigate the re-covery of catalytic activity. The fixed-bed quartz reactor was filled in with 1.2 mL of the thermally-deactivated material (FeTi-T). The gas mixture (1200 mL/min) containing NO (600 ppm), NH_3 (600 ppm), H_2O (4.0%), O_2 (4.0%) and SO_2 (1000 ppm) in N_2 was introduced into the reactor at 350 °C for approximately 30 h to yield the regenerated material (FeTi-S). Concentrations of NO and NO_2 in the outlet were

detected by a T-340 flue gas analyzer.

2.4. Catalyst characterizations

N_2 adsorption-desorption was conducted at −196 °C using a Quantachrome NOVA 2000e surface area and pore size analyzer. The sample was first degassed under vacuum at 300 °C for 3 h. The Brunauer-Emmett-Teller (BET) method was subsequently used to cal-culate the specific surface area of each material. Powder XRD of each material was conducted using a PANalytical B.V. X'Pert Pro XRD dif-fractometer with Cu Kα radiation and the X-ray tube was operated at 40 kV and 40 mA. TGA was carried out on a HCT-1 thermoanalyzer (Beijing Hengjiu Company, China) in a flowing N_2. The heating rate was 10 °C/min. FTIR was conducted on a Bruker Vertex 70 infrared spec-trometer with a resolution of 4 cm^{-1} (64 scans). XPS was performed on a Thermo Fisher Scientific ESCALAB 250 spectrometer, using Al Kα radiation. The binding energy of each material was compensated with the adventitious C 1 s peak at 284.6 eV. H_2-TPR was performed on a Quantachrome ChemBET-3000 TPR-TPD chemisorption analyzer using a gas feed of 5% H_2/Ar. Before switching to the H_2/Ar feed, the sample (50 mg) was pretreated under a helium flow at 400 °C for 1 h. During the TPR experiment, the temperature was progressively increased from 50 to 900 °C at a rate of 10 °C/min. An online mass spectrometer (MS, DYCOR LC-D100, Ametek Company, USA) was used as the detector·NH_3-TPD was also performed on the ChemBET-3000 TPR-TPD chemisorption analyzer with an on-line MS as detector. For this, each sample (50 mg) was pretreated under flowing helium at 400 °C for 1 h and then cooled to 50 °C. After that, 5% NH_3/Ar was introduced for 30 min and then the carrier gas was switched to helium. To remove any weakly adsorbed NH_3 from the surface of the material, the material was purged with helium at 100 °C for 1 h. The temperature was then in-creased to 600 °C at a ramp rate of 10 °C/min. In situ DRIFTS was per-formed on a Bruker Vertex 70 infrared spectrometer with a MCT de-tector. A Harrick Scientific reaction cell with ZnSe windows was used. The powdered sample in the reaction cell was first treated under N_2 at 400 °C for 1 h and then cooled to 350 °C. Background spectra were re-corded at 350 °C. Afterwards, the target mixture gas was introduced and the spectrum was recorded at a given time by 100 scans with a re-solution of 4 cm^{-1}.

2.5. Calculation methods

The first-principle density functional theory calculations (including structural and electronic investigations) were conducted based on the Cambridge Sequential Total Energy Package (CASTEP) and used to investigate the adsorption of SO_2 and NH_3 on the catalyst model. The model of TiO_2 (0 0 1) surfaces was used because the stability of (0 0 1) surfaces of anatase TiO_2 was the lowest and should play an important role in catalytic reaction [30]. More details could be found in our previous work [32,33].

3. Results and discussion

3.1. NO_x conversion over catalysts

NO_x conversion observed over all prepared samples is displayed in Fig. 1a. The FeTi material exhibited an exceptionally high catalytic activity with over 90% of NO_x converted between 350 and 450 °C, in line with previous reports [19]. A significant decrease of catalytic ac-tivity was observed over FeTi-T material, suggesting that the thermal treatment had a negative effect on the activity of $Fe_2(SO_4)_3/TiO_2$ cat-alyst. For FeTi-T material, NO_x conversion was found to be lower than 70% at all the temperatures. The catalytic activity of FeTi-S material was subsequently investigated and a significant increase in the con-version of NO_x was observed. The catalytic activity was found to be comparable with that of FeTi material. N_2O is an important greenhouse gas and it's the main by-product of NH_3-SCR reaction [34]. The N_2 selectivity of prepared materials is shown in Fig. 1a. The N_2 selectivity was higher than 98% within the test temperatures for FeTi material, in accordance with other researches [19]. After the thermal treatment, the N_2 selectivity showed a significant decrease. However, N_2 selectivity recovered after FeTi-T material was sulfated by SO_2.

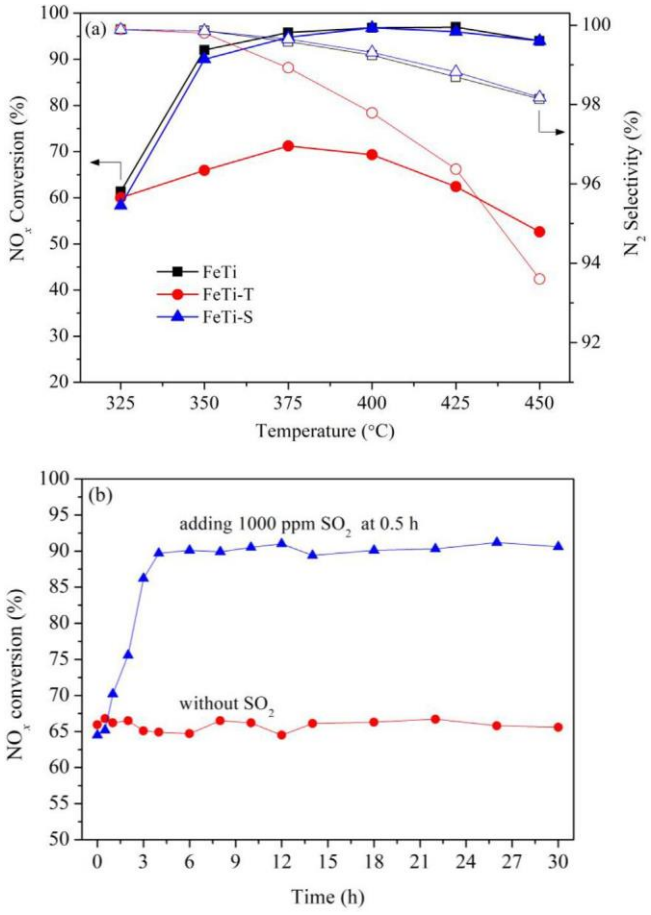

Fig. 1. (a) NO_x conversion and N_2 selectivity of the prepared catalysts. (b) Time-on-stream NO_x conversion of FeTi-T catalyst with and without SO_2 at 350 °C. (Reaction conditions: GHSV = 60 000 h^{-1}, [NO] = [NH_3] = 500 ppm, [H_2O] = 4.0%, [O_2] = 4.0%).

The time-on-stream data for the activity recovery experiment is displayed in Fig. 1b. The addition of SO_2 into the gas mixture at 350 °C resulted in a noticeable increase of the NO_x conversion over FeTi-T material; NO_x increased rapidly from 65% to 90% after only 2.5 h and remained stable until the end of the experiment. By comparison, the NO_x conversion observed over FeTi-T material (in the absence of SO_2) only reached and maintained at 65% across the test period. It can therefore be concluded that the thermal pre-treatment causes the de-activation of the $Fe_2(SO_4)_3/TiO_2$ catalyst. It was also clear that flowing SO_2 over this material leads to a recovery in its catalytic performance.

3.2. Characterization of synthesized catalysts

3.2.1. Structural and surface properties

Table 1 shows the specific surface area (S_{BET}), total pore volume (V_p) and average pore diameter (D_p) of each material. The S_{BET} and D_p of $Fe_2(SO_4)_3/TiO_2$ catalyst was 64.3 m^2/g and 7.5 nm, respectively. After the thermal treatment under N_2, a significant structural change in the $Fe_2(SO_4)_3/TiO_2$ catalyst occurred; the S_{BET} decreased from 64.3 to 54.1 m^2/g with the D_p increased from 7.5 to 8.5 nm. The sintering of the carrier might occur under the thermal treatment and thus caused the

Table
Physico-chemical properties of each catalyst.

Sample	S_{BET} (m^2/g)	V_p[a] (cm^3/g)	D_p (nm)	d_{crys}[b] (nm)	T_{acid}[c] (mmol/g)
F	6				
FeTi	5				
FeT	5				

[a] Obtained at $P/P_0 = 0.99$.

[b] Calculated by the Scherrer formula based on the (1 0 1) plane of anatase TiO_2 in XRD patterns.

[c] Calculated by the integral area of the desorption peak in NH_3-TPD.

reduction of specific surface area. After sulfation by SO_2, the S_{BET} of FeTi-T material did not appear to decrease significantly, indicating that the sulfation had little effect on the carrier. In general, the decrease of the specific surface area could cause the deactivation of catalysts. The S_{BET} of FeTi-S material was significantly lower than that of FeTi ma-terial; however, their catalytic activities were almost the same. There-fore, it could be concluded that the decrease of the specific surface area should not be the main reason for the deactivation of the catalyst after thermal treatment.

XRD patterns of all the materials are displayed in Fig. 2. The most intense diffraction peaks observed on FeTi material corresponded to anatase TiO_2 and diffraction peaks associated with $Fe_2(SO_4)_3$ phases were very weak, suggesting that the $Fe_2(SO_4)_3$ species were likely to be well dispersed on TiO_2 support. After the thermal treatment, however, the diffraction peaks associated with $Fe_2(SO_4)_3$ disappeared completely and diffraction peaks corresponded to α-Fe_2O_3 phase were observed, suggesting that significant quantities of the $Fe_2(SO_4)_3$ decomposed during the heat treatment according to Eq. (3). In addition, there were no obviously peaks assigned to rutile TiO_2, suggesting that the phase transitions from anatase to rutile might not occur. For FeTi-S material, new small diffraction peaks associated with $Fe_2(SO_4)_3$ were observed, implying that $Fe_2(SO_4)_3$ could be recovered according to Eq. (4). The average crystallite size of anatase TiO_2 (d_{cry}) is often used to determine the degree of TiO_2 sintering at high temperatures [23,24]. The d_{cry} of each material was calculated using the Scherrer equation based on full width at half maximum (FWHM) of the TiO_2 (1 0 1) plane, the results of which are also displayed in Table 1. The d_{cry} associated with FeTi material was calculated to be 21.7 nm, which was similar to the results reported in the literature [23,24]. After the thermal treatment, the d_{cry} of FeTi-T material increased to 24.3 nm, suggesting that the sintering of anatase TiO_2 occurred, which also aligned with the decrease observed in the S_{BET}.

$$2Fe_2(SO_4)_3 \rightarrow 3Fe_2O_3 + 6SO_2 + 3O_2$$

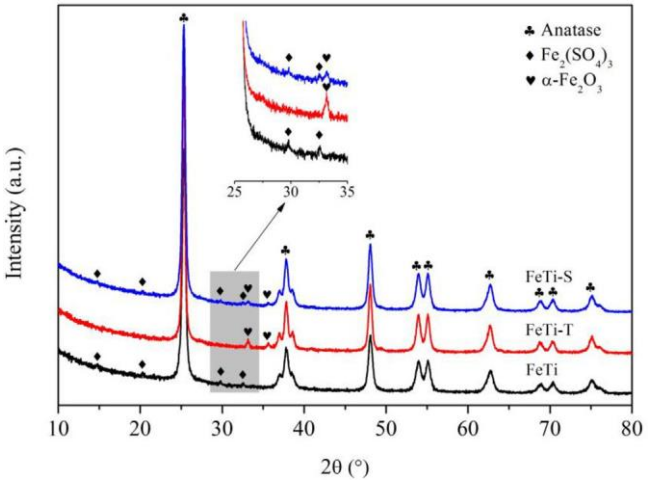

Fig. 2. XRD results of prepared catalysts.

$$2Fe_2(SO_4)_3 + 6SO_2 + 3O_2 \rightarrow 2Fe_2(SO_4)_3 \quad (4)$$

TGA was subsequently used to assess the mass loss of all materials, as shown in Fig. S1. For FeTi material, the mass loss started from 400 °C and a mass loss of 5.5% was observed at approximately 850 °C, while a mass loss of only 0.5% was observed for FeTi-T material. This indicated that a significant proportion of the $Fe_2(SO_4)_3$ was likely to have de-composed during the thermal treatment, in accordance with the con-clusions drawn from the XRD (Fig. 2). Interestingly, after FeTi-T ma-terial was subjected to the activity recovery step, an increase in the quantity of mass loss in the TGA was observed (4.0% for FeTi-S mate-rial). Most of $Fe_2(SO_4)_3$ should be recovered, according to Eq. (4).

The FTIR spectra of prepared materials are shown in Fig. S2. A board peak in the range from 900 to 400 cm^{-1} and three peaks at 1221, 1136, 1045 cm^{-1} could be found on $Fe_2(SO_4)_3/TiO_2$ catalysts. The board peak could be associated with anatase TiO_2 and those three peaks could be associated with the stretching motion of adsorbed HSO_4^- and SO_4^{2-} on the surface of the catalyst [35,36]. After the thermal treat-ment, the board peak split into two peaks centered at 702 and 521 cm^{-1}, respectively, indicating that the sintering of TiO_2 carrier occurred, in accordance with the results of XRD and other researches [36]. The three peaks assigned to adsorbed HSO_4^- and SO_4^{2-} almost disappeared, suggesting that most of the $Fe_2(SO_4)_3$ decomposed on FeTi-T material. However, the three peaks were largely recovered on FeTi-S material, suggesting that most of sulfate should recover after the sulfation, in accordance with the results of XRD and TGA.

XPS was subsequently used to determine the chemical states of Fe, Ti, O and S in prepared materials, as displayed in Fig. 3. An intense peak could be observed in all materials at a binding energy of around 711.4 eV, which suggested that iron predominantly existed in a Fe^{3+} state [37]. In the XPS spectrum of FeTi material, two peaks at 459.0 and 464.7 eV were also observed and could be attributed to the spin-split orbits components of Ti 2p. From the XPS spectrum of this material after the thermal treatment, both of these peaks appeared to have shifted to 459.4 and 465.0 eV, which was further evidence to suggest that the thermal treatment facilitated the sintering of TiO_2. It is re-ported that the sintering could increase the size of TiO_2 nanoparticles and thus caused the peaks shift to higher binding energies to some extent [38]. For all synthesized materials, O 1 s curves could be fitted into three peaks, which respectively assigned to the lattice oxygen (O_α), surface OH group (O_β) and weakly adsorbed oxygen (O_γ, Table 2) [39–41]. For FeTi material, O_β of the total oxygen was 43.4%. After the thermal treatment, the ratio of O_β decreased largely (12.4%) on FeTi-T material, suggesting that the thermal treatment would cause the dis-appearance of a large number of surface OH group. Most of surface OH

(3) group recovered after sulfation and the O_β increased to 39.4%. Surface OH group could supply Brønsted acid sites on the surface of catalysts and benefit the occurrence of NH_3-SCR reaction [20,42]. The recovery of surface OH group should be one of the main reasons for the activity recovery of the deactivated catalysts. In the S 2p region of the spectrum, a large peak at 168.4 eV (indicative of HSO_4^- species) and a shoulder peak at 169.8 eV (indicative of SO_4^{2-} species) was observed on FeTi material [43]. After the thermal treatment, the intensity of S 2p peaks decreased significantly and the peak assigned to HSO_4^- species almost disappeared. Only a small peak at 169.3 eV assigned to SO_4^{2-} could be found, suggesting that a large proportion of the sulfate especially hydrosulfate species on the surface of the catalyst decomposed during the thermal treatment, which correlated well with the conclusions drawn from XRD, TGA and FTIR (Figs. 2, S1 and S2). Upon exposure to SO_2 however, the intensity of S 2p peaks increased once again, suggesting that the activity recovery step led to formation of sulfate and hydro-sulfate species on the surface of the material. As Fig. 3 showed, the shape of Fe 2p3/2 and S 2p for FeTi-S sample was similar to the shape of FeTi sample, thus we concluded that most of $Fe_2(SO_4)_3$ should be recovered after the sulfation, be in line with the results of XRD, TGA and FTIR.

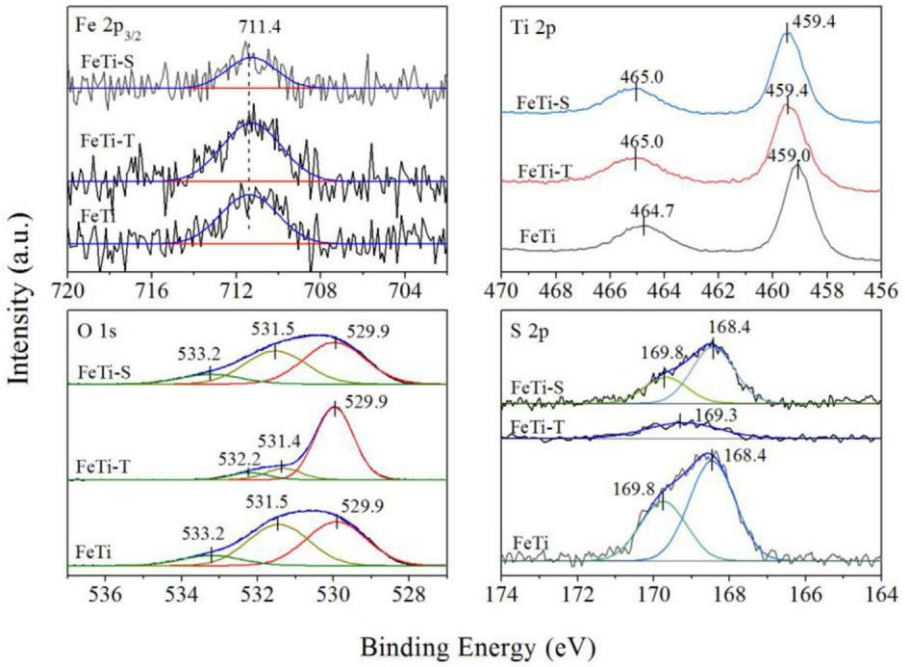

Fig. 3. XPS results of Fe 2p3/2, Ti 2p, O 1 s and S 2p for prepared materials.

Table 2
The content of O and S species in different catalysts.

Sample	O 1 s			S 2p	
	Oα (%)	Oβ (%)	Oγ (%)	Sα (%)	Sβ (%)
FeTi	46.0 (529.9)	43.4 (531.5)	10.6 (533.2)	37.8 (168.4)	62.2 (169.8)
FeTi-T	79.8 (529.9)	12.4 (531.4)	7.8 (532.2)	/	100 (169.3)
FeTi-S	49.1 (529.9)	39.4 (532.2)	11.5 (533.2)	35.7 (168.4)	64.3 (169.8)

[a] Oα: lattice oxygen, Oβ: surface OH group, Oγ: adsorbed oxygen; Sα: HSO_4^-, Sβ: SO_4^{2-} (Data in parentheses means the position of the peak (eV)).

3.2.2. Reducibility and surface acidity

Previous works have proved that the surface reducibility can affect the activity of SCR catalysts [44,45]. For this reason, H_2-TPR was used to determine the effect the thermal treatment on surface reducibility of the catalyst. The corresponding data for these experiments is displayed in Fig. 4. A broad H_2 (m/e = 2) consumption peak was observed in H_2-TPR of FeTi material between the temperatures of 400 and 650 °C (centered at 565 °C). The release of H_2S, SO_2 and SO_3 during H_2-TPR process was also measured by MS and only the signal of SO_2 (m/e = 64) could be detected (Fig. 4). It was determined that the emission of SO_2 occurred almost in parallel with the H_2 consumption, suggesting that the H_2 consumption was likely indicative of $Fe_2(SO_4)_3$ reduction ac-cording to Eq. (5) and was in line with reports from previous publica-tions [20]. The H_2 consumption peak of FeTi-T material shifted to 510 °C and the intensity decreased significantly, which was likely at-tributed to the presence of α-Fe_2O_3 (Eq. (6)) (confirmed by XRD). As Eqs. (5) and (6) showed, the H_2 consumption quantity over Fe_2O_3 was smaller than that of $Fe_2(SO_4)_3$. In addition, a much smaller quantity of SO_2 was emitted for FeTi-T material. After exposure to SO_2 (FeTi-S material), a boarder H_2 consumption peak centered at 554 °C was presented and the release of SO_2 increased significantly, providing further evidence to suggest that the activity recovery procedure fa-cilitated the production of new $Fe_2(SO_4)_3$.

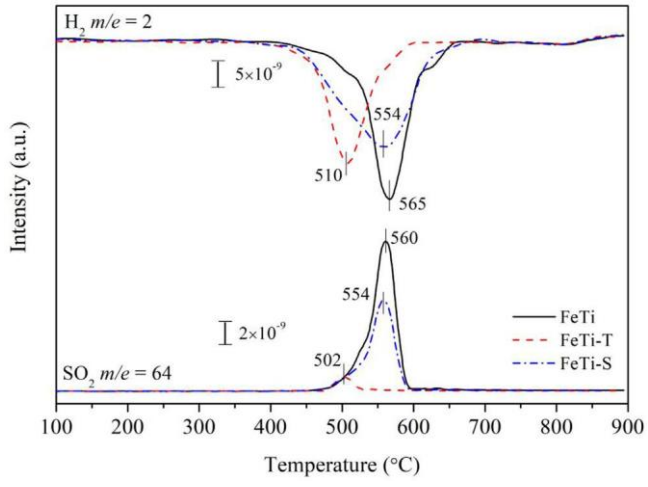

Fig. 4. H_2-TPR profiles and the release of SO_2 during H_2-TPR for synthesized materials.

$$Fe_2(SO_4)_3 + 6H_2 \rightarrow 2Fe + 3SO_2 + 6H_2O \quad (5)$$

$$Fe_2O_3 + 3H_2 \rightarrow 2Fe + 3H_2O \quad (6)$$

Typically, in NH_3-SCR reactions, the absorption of NH_3 onto the surface acid sites is considered to be one of the key steps in the reaction [46–48]. In order to determine how the thermal treatment affected this, NH_3-TPD was conducted on all materials (Fig. 5). NH_3 desorption on FeTi material began at approximately 100 °C and ended at approxi-mately 600 °C with the total amount of acid sites (T_{acid}) calculated to be approximately 0.352 mmol/g. After the thermal treatment, the T_{acid} decreased significantly and was calculated to be approximately 0.072 mmol/g (20% of that observed over FeTi material). After the subsequent exposure to SO_2, the T_{acid} increased to 0.274 mmol/g (78% of that observed over FeTi material). It can be therefore concluded that the thermal treatment caused a decrease in the amount of acid sites on the surface of the catalyst and that the sulfation step partly facilitated the recovery of some acid sites.

In situ DRIFTS was subsequently used to investigate the nature of the acid sites on each material. The DRIFTS spectra depicting the adsorp-tion of NH_3 onto each material at 350 °C are displayed in Fig. 6. Several bands were observed in the spectrum of FeTi material after exposure to

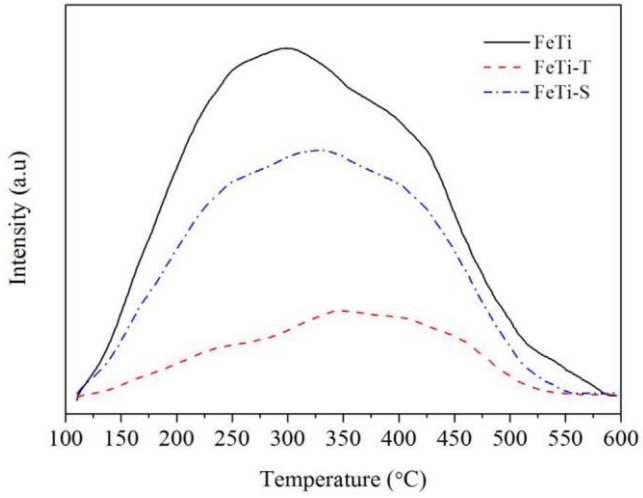

Fig. 5. NH_3-TPD profiles of prepared materials.

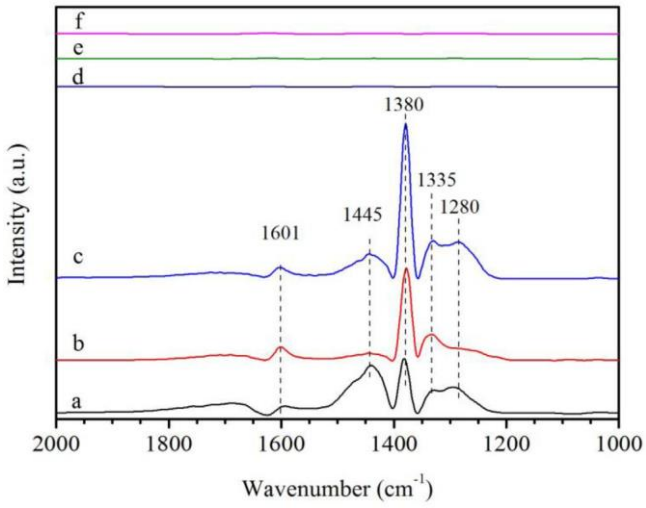

Fig. 6. DRIFTS spectra corresponding to the adsorption of NH_3 (a-c) and NO + O_2 (d–f) on various samples at 350 °C. (a, d: FeTi material; b, e: FeTi-T material; c, f: FeTi-S material).

NH_3 for 15 min and purged with N_2 for another 10 min. The band at 1445 cm^{-1} and the broad band from 1635 to 1850 cm^{-1} were assigned to NH_4^+ species chemisorbed onto Brønsted acid sites [49,50]. The band at 1601 cm^{-1} was indicative of NH_3 adsorbed onto Lewis acid sites [49,50]. The bands at 1380, 1335 and 1280 cm^{-1} were attributed to NH_2 wagging [51,52]. The thermal treatment of FeTi material did not appear to have a significant effect on Lewis acid sites as no sig-nificant change was observed for the band at 1601 cm^{-1}. A significant reduction in intensity however, was observed for the bands at 1445 cm^{-1} and 1635–1850 cm^{-1} suggesting that the thermal treatment led to a loss of Brønsted acid sites on the material. This was likely due to the decomposition of $Fe_2(SO_4)_3$, as the presence of SO_4^{2-} and HSO_4^- on the surface formed Brønsted acid sites according to previous reports [20]. Brønsted acid sites play a key role in NH_3-SCR reactions for sulfate catalysts [42,53]. For NH_3-SCR reaction, NH_3 is first absorbed on sur-face Brønsted acid sites and then reacted with NO and O_2 to form N_2 and H_2O. The thermal treatment caused the decomposition of $Fe_2(SO_4)_3$ on $Fe_2(SO_4)_3/TiO_2$ catalysts and thus most of the Brønsted acid sites disappeared, which hindered the adsorption and activation of NH_3 on the surface of the catalyst, as shown in Scheme 1a. The loss of Brønsted acid sites were likely to be the main reason why such a significant loss in activity was observed after the thermal deactivation. The bands associated with chemisorbed NH_4^+ onto Brønsted acid sites reemerged on FeTi-S material, providing further evidence that the activity re-covery procedure in the presence of SO_2 assisted with the reformation of some of the Brønsted acid sites.

The adsorption of NO was also detected by in situ DRIFTS and the results can be found in Fig. 6. It can be found that NO was hardly ad-sorbed on the surface of prepared materials at 350 °C. The influence of SO_2 on the adsorption of NH_3 over FeTi-T material was also in-vestigated and the corresponding results are displayed in Fig. S3. It is clear that the intensity of both the band at 1445 cm^{-1} and the broad band from 1635 to 1850 cm^{-1} increased with the exposure time, sug-gesting that Brønsted acid sites are formed in situ on the surface of the material in the presence of SO_2.

The interaction between NO/O_2 and NH_3 pre-adsorbed on FeTi and FeTi-S materials was investigated at 350 °C and the results can be found in Figs. S4 and S5. After NO and O_2 were introduced, bands assigned to NH_3 adsorbed on FeTi material decreased significantly and almost disappeared after 2 min. A new band at 1624 cm^{-1} indicative of a bridging nitrate species and a small band at 1345 cm^{-1} indicative of a surface NO_3^- species appeared [54,55]. However, both these bands almost disappeared after purging with N_2 for 15 min, implying that the bridging nitrate and surface NO_3^- species were unstable at 350 °C. It is likely that the surface reaction mechanism on $Fe_2(SO_4)_3/TiO_2$ catalysts proceeds via an Eley-Rideal surface mechanism·NH_3 was absorbed onto the surface of catalyst and then reacted with NO and O_2, forming N_2 and H_2O. To investigate whether the same surface mechanism occurred on FeTi-S material, a same in situ DRIFTS experiment was conducted. The in situ DRIFTS experiment conducted over FeTi-S material yielded very similar results, suggesting that the newly formed Brønsted acid sites participate in the reaction in the same way as the Brønsted acid sites in the fresh FeTi catalyst. It was therefore highly likely that the surface mechanism that took place on both FeTi-S and FeTi materials was the same. As such, we can conclude that the new Brønsted acid sites formed from exposing FeTi-T material to SO_2 are likely to be the main reason why the recovery of catalytic activity is observed.

3.2.3. In situ DRIFTS of FeTi-T material under $SO_2 + O_2$

The co-adsorption of SO_2 and O_2 on FeTi-T was also investigated by in situ DRIFTS. The results from this investigation are displayed in Fig. 7a. After exposure to SO_2 and O_2 for 30 min, bands at 1370, 1298 and 1170 cm^{-1} were observed. The bands at 1370 and 1298 cm^{-1} were indicative of the asymmetric vibrations of surface sulfate species with covalent O]S]O [11,56]. The band at 1170 cm^{-1} was indicative of bulk sulfate species [11], suggesting that both surface and bulk sulfate species were formed in the presence of SO_2 and O_2. The sample was subsequently purged by N_2 for another 15 min and then exposed to NH_3 (Fig. 7b). Interestingly, the peaks associated with surface and bulk sulfate species were still detected after purged by N_2, suggesting that most of the newly formed sulfate species was stable. According to previous research, SO_2 can be adsorbed on TiO_2 as $(Ti\text{-}O)_3$ S]O and would give two peaks of roughly equal intensity at 1367–1381 and 1386–1408 cm^{-1}, respectively [57]. However, we can only find one peak at 1370 cm^{-1} from Fig. 7a. F. Liu et al. [29] studied the adsorption of SO_2/O_2 on Fe_2O_3 and they found a peak at 1372 cm^{-1} from in situ DRIFTS and the peak was indicative of the sulfate species formed on iron sites in a chelating bidentate conformation. It can be concluded that the bidentate sulfate on Fe atoms should be formed in the thermal deactivated $Fe_2(SO_4)_3/TiO_2$ catalyst after treated by SO_2 and O_2.

After pretreated by SO_2/O_2 and purged by N_2, NH_3 was introduced and the bands at 1445 cm^{-1} and the broad band at 1635–1850 cm^{-1} were detected (Fig. 7b), providing evidence for the existence of Brønsted acid sites on the material after the treatment with SO_2 and O_2. As such, we can conclude that the exposure of FeTi-T material to SO_2 reforms sulfate species on the surface of materials which ultimately leads to the regeneration of Brønsted acid sites. The proposed pathway for formation of Brønsted acid sites on FeTi-S material can be found in

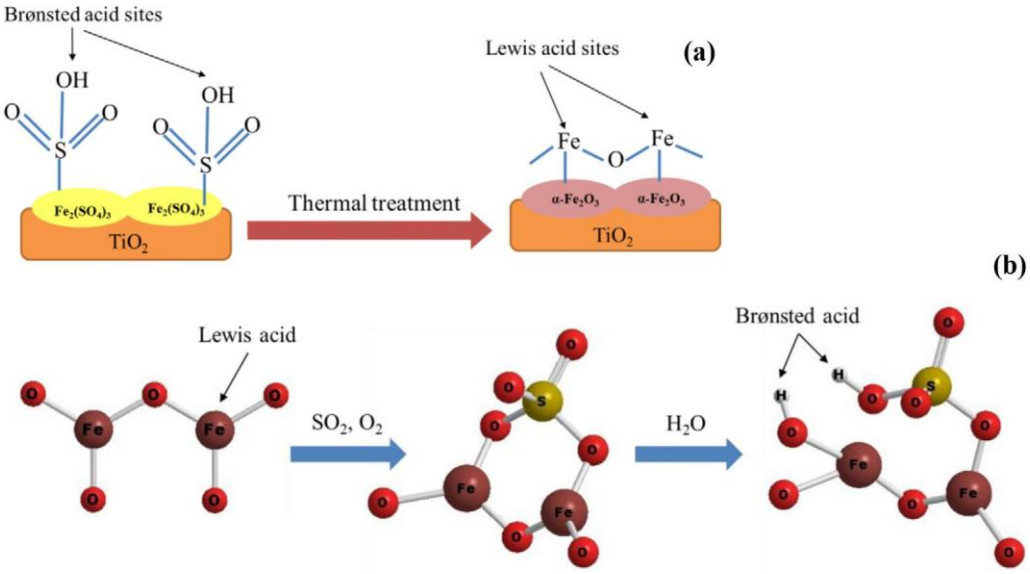

Scheme 1. (a) The influence of thermal treatment on the Brønsted acid site over $Fe_2(SO_4)_3/TiO_2$ catalyst; (b) The proposed pathway for formation of Brønsted acid sites on FeTi-S material.

Scheme 1. Due to the electron-withdrawing oxygen groups, the partial positive charge created on Fe atom formed Lewis acid sites. After sul-fated by SO_2 and O_2, the bidentate sulfates were formed on Fe atoms. Then the Brønsted acid sites were generated by interaction of water with surface bidentate sulfates.

3.3. DFT calculations

According to previous researches, the stability of (0 0 1) surfaces of anatase TiO_2 was the lowest and should play an important role in catalytic reaction [30], thus the model of TiO_2 (0 0 1) surfaces has been used by many researchers in DFT calculations. The optimized model of Fe_2O_3 bonded to TiO_2 (0 0 1) surface was calculated firstly and can be found in Fig. 8a. The bond length of Fe-O was 1.700 Å and the bond length of O-Fe-O was range from 1.721 to 1.759 Å. Then the adsorption of SO_2 on the Fe_2O_3/TiO_2 model was calculated (Fig. 8b). It could be found that SO_2 was preferential adsorbed on Fe_2O_3 via Fe-S (the bond length was 2.129 Å) and S-O (the bond length was 2.429 Å). The ad-sorption of SO_2 also affected the configuration parameter of Fe_2O_3. The bond length of Fe-O increased to 1.711 Å and the bond length of O-Fe-O decreased to 1.708 Å. The electron density difference (EDD) map can characterize the electron accumulation and loss of atoms and EDD map of SO_2 adsorption can be found in Fig. 8c. In the EDD map, electron accumulation was showed by the red and yellow regions and electrons loss was showed by blue and green regions. The color between S and Fe atoms was red, suggesting that the electron accumulation between S and Fe atoms was very high, thus S atom was easy to form chemical bond with Fe atom, further proving that SO_2 was preferential adsorbed on Fe_2O_3 of FeTi-T material. The S atom would loss electron after the adsorption of SO_2 on Fe_2O_3, which could lead to the increase of che-mical valence of S atom, in consistent with the results of XPS. As Fig. 3 showed, the highest valence of S (S^{6+} from HSO_4^- and SO_4^{2-}) was the main S species. It can be concluded that the sulfate on FeTi-S material should mainly unite with Fe species from the results of DFT calcula-tions, in accordance with the results of in situ DRIFTS.

The adsorption of NH_3 on each model was then calculated and the results are shown in Fig. 9. For the Fe_2O_3/TiO_2 model, it can be found NH_3 should be adsorbed on Fe_2O_3 via Fe-N and the adsorption energy was −2.12 eV. When NH_3 was adsorbed on sulfated Fe_2O_3/TiO_2 model, it can be found that the adsorption of NH_3 had a large influence on the SO_2 adsorption: the S-Fe bond was broken and SO_2 adsorbed on Fe_2O_3 via S-O bond·NH_3 was adsorbed on the top of SO_2 via N-S bond and the adsorption energy was −1.11 eV. Thus, it can be concluded that the

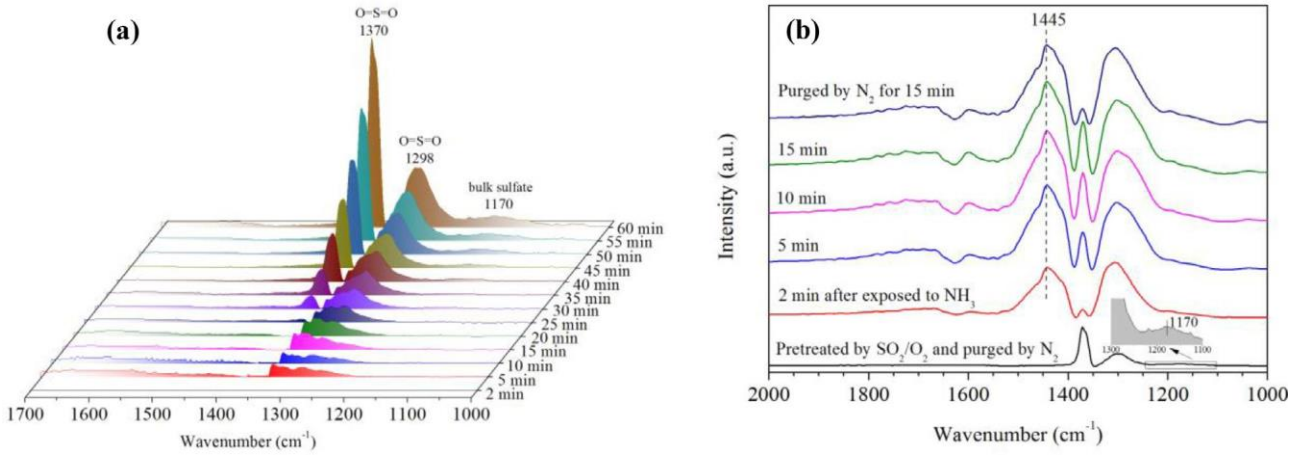

Fig. 7. DRIFTS spectra corresponding to (a) the co-adsorption of SO_2 and O_2 on the FeTi-T material and (b) the adsorption of NH_3 on the FeTi-T material pretreated by SO_2 and O_2. All spectra were collected at 350 °C.

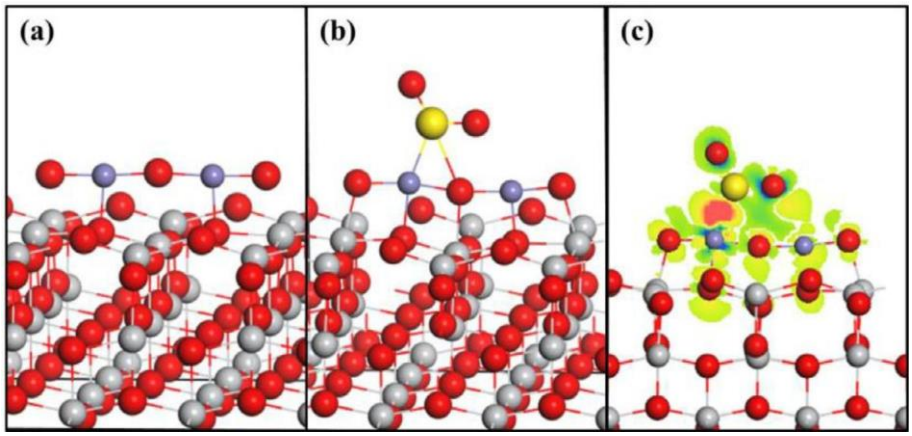

Fig. 8. Optimized structures of (a) Fe_2O_3/TiO_2, (b) SO_2 adsorbed on Fe_2O_3/TiO_2 and (c) EDD map of SO_2 adsorbed on Fe_2O_3/TiO_2 (Red ball: O atom; Gray ball: Ti atom; Light blue ball: Fe; atom; Yellow ball: S atom).

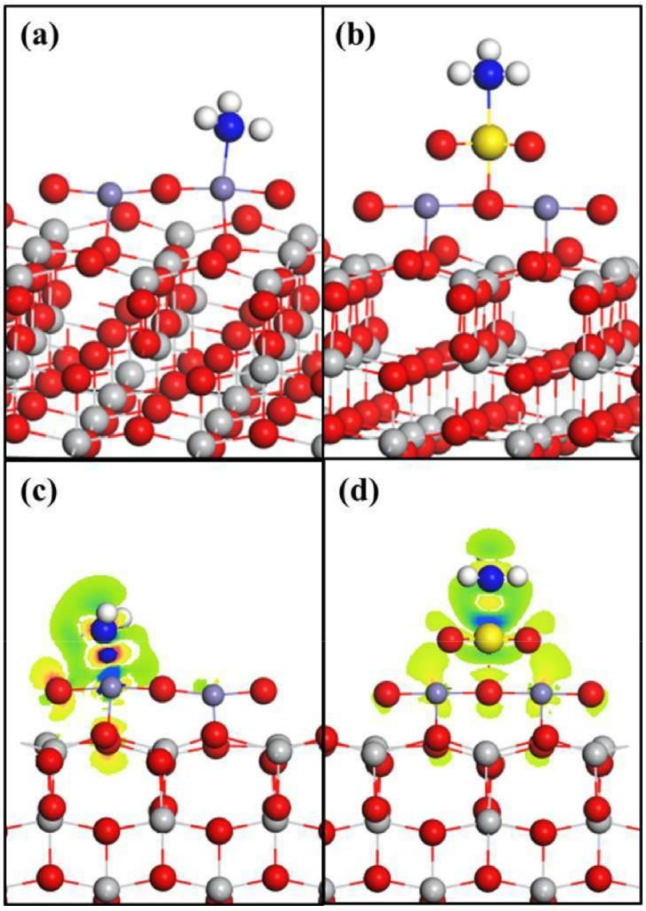

Fig. 9. Optimized structures for NH_3 adsorption on (a) Fe_2O_3/TiO_2, (b) Sulfated Fe_2O_3/TiO_2 and (c, d) corresponding EDD maps (Red ball: O atom; Gray ball: Ti atom; Light blue ball: Fe; atom; Yellow ball: S atom; Dark blue ball: N atom; White ball: H atom).

newly formed sulfate should be the main sites for NH_3 adsorption, in accordance with the results of in situ DRIFTS.

Projected density of states (PDOS) analysis can be used to under-stand the interaction and nature bonding between SO_2 and surface atoms [58,59]. The total PDOS of the system could be found in Fig. S6, it could be found that the total PDOS was mainly composed of p- and d-orbitals in the energy level range. Following this, the PDOS results of S and Fe atoms were further analyzed (Fig. 10). The degree of over-

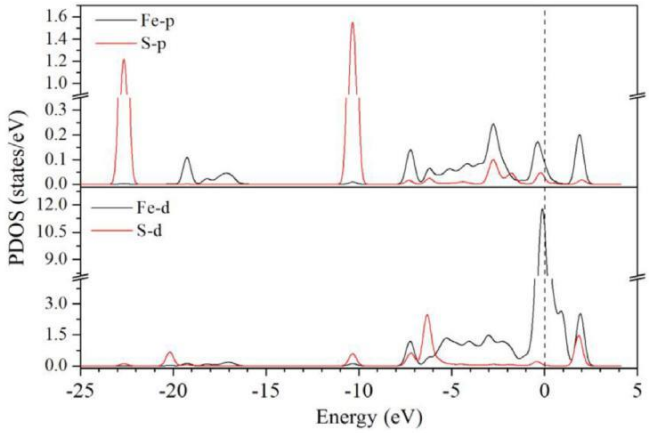

Fig. 10. PDOS analysis of Fe and S orbitals of sulfated Fe_2O_3/TiO_2.

lapping between the density peaks and their position with respect the Fermi level (0 eV) was usually used to analyze the bonding strength between adsorbate and surface atoms [58,59]. As Fig. 10 showed, the degree of over-lapping in p orbitals for S and Fe atoms was very high, indicating that the orbital hybridization between O and Fe atoms oc-curred and there was a strong interaction between S and Fe atoms. S-p orbital presented the same density peak positions at −2.9, −6.1, −7.1 and −10.4 eV below the Fermi level as Fe-p orbital. Compared with p orbital, the over-lapping in d orbital showed a lower degree and the over-lapping position was further from the Fermi level, suggesting that S-Fe bond should mainly formed by electrons from p orbitals of S and Fe atoms.

4. Conclusions

The exposure of $Fe_2(SO_4)_3/TiO_2$ catalyst to high temperatures leads to decomposition of $Fe_2(SO_4)_3$, thus causes a significant reduction of Brønsted acid sites on the surface of the material. This reduction in Brønsted acidity correlates with a reduction in the NO_x conversion, indicating that the Brønsted acid sites play an important role in the catalytic conversion of NO_x. Interestingly, exposing this thermally-de-activated catalyst to SO_2 under the standard reaction conditions leads to the recovery of most $Fe_2(SO_4)_3$ and the regeneration of some of the Brønsted acid sites on the material surface and ultimately increases the catalytic performance to the level observed with the fresh catalyst. Given that many industrial flue gas streams contain SO_2, sulfate cata-lysts such as the one used in this study offer a stable and highly active alternative to conventional vanadium-based catalysts for industrial

NH_3-SCR applications. We hope that this work will provide a founda-tion for further investigations into sulfate vanadium-free SCR catalysts.

Acknowledgements

We gratefully acknowledge the financial support from the National Natural Science Foundation of China (21477095, 21677114, 21876139), the National Key Research and Development Program (2016YFC0204201), the Natural Science Foundation of Fujian Province, China (2016J05048), the General Financial Grant from the China Postdoctoral Science Foundation (2016M602831), and the Fundamental Research Funds for the Central Universities (xjj2017113). We thank Ms. Cun Deng and Jiamin Wu (undergraduate students from XJTU) for their helpful work on activity measurement, and valuable comments from the editor and anonymous reviewers are much appre-ciated.

Appendix A. Supplementary data

Supplementary data to this article can be found online at https://doi.org/10.1016/j.cej.2018.12.149.

References

[1] X. Li, K. Li, Y. Peng, X. Li, Y. Zhang, D. Wang, J. Chen, J. Li, Interaction of phos-phorus with a $FeTiO_X$ catalyst for selective catalytic reduction of NO_X with NH_3: Influence on surface acidity and SCR mechanism, Chem. Eng. J. 347 (2018) 173–183.

[2] M. Zhu, J. Lai, U. Tumuluri, Z. Wu, I.E. Wachs, Nature of active sites and surface intermediates during SCR of NO with NH_3 by supported V_2O_5-WO_3/TiO_2 catalysts, J. Am. Chem. Soc. 139 (2017) 15624–15627.

[3] F. Liu, W. Shan, Z. Lian, J. Liu, H. He, The smart surface modification of Fe_2O_3 by WO_X for significantly promoting the selective catalytic reduction of NO_X with NH_3, Appl. Catal., B 230 (2018) 165–176.

[4] L. Zheng, M. Zhou, Z. Huang, Y. Chen, J. Gao, Z. Ma, J. Chen, X. Tang, Self-pro-tection mechanism of hexagonal WO_3-based $DeNO_X$ catalysts against alkali poi-soning, Environ. Sci. Technol. 50 (2016) 11951–11956.

[5] Y. Li, X. Han, Y. Hou, Y. Guo, Y. Liu, Y. Cui, Z. Huang, Role of CTAB in the improved H_2O resistance for selective catalytic reduction of NO with NH_3 over iron titanium catalyst, Chem. Eng. J. 347 (2018) 313–321.

[6] F. Gao, D. Mei, Y. Wang, J. Szanyi, C.H. Peden, Selective catalytic reduction over Cu/SSZ-13: Linking homo-and heterogeneous catalysis, J. Am. Chem. Soc. 139 (2017) 4935–4942.

[7] T. Ryu, N.H. Ahn, S. Seo, J. Cho, H. Kim, D. Jo, G.T. Park, P.S. Kim, C.H. Kim, E.L. Bruce, Fully copper-exchanged high-silica LTA zeolites as unrivaled hydro-thermally stable NH_3-SCR catalysts, Angew. Chem. Int. Ed. 56 (2017) 3256–3260.

[8] X. Tang, C. Li, H. Yi, L. Wang, Q. Yu, F. Gao, X. Cui, C. Chu, J. Li, R. Zhang, Facile and fast synthesis of novel Mn_2CoO_4@rGO catalysts for the NH_3-SCR of NO_X at low temperature, Chem. Eng. J. 333 (2018) 467–476.

[9] P. Wang, S. Chen, S. Gao, J. Zhang, H. Wang, Z. Wu, Niobium oxide confined by ceria nanotubes as a novel SCR catalyst with excellent resistance to potassium, phosphorus, and lead, Appl. Catal., B 231 (2018) 299–309.

[10] Y. Peng, D. Wang, B. Li, C. Wang, J. Li, J.C. Crittenden, J. Hao, Impacts of Pb and SO_2 poisoning on CeO_2-WO_3/TiO_2-SiO_2 SCR catalyst, Environ. Sci. Technol. 51 (2017) 11943–11949.

[11] K. Qi, J. Xie, H. Hu, D. Han, D. Feng, P. Gong, F. Li, F. He, X. Liu, Facile synthesis of Mn-based nanobelts with high catalytic activity for selective catalytic reduction of nitrogen oxides, Chem. Eng. J. 352 (2018) 39–44.

[12] W. Shan, H. Song, Catalysts for the selective catalytic reduction of NO_X with NH_3 at low temperature, Catal. Sci. Technol. 5 (2015) 4280–4288.

[13] F. Gao, X. Tang, H. Yi, J. Li, S. Zhao, J. Wang, C. Chu, C. Li, Promotional me-chanisms of activity and SO_2 tolerance of Co- or Ni-doped MnO_X-CeO_2 catalysts for SCR of NO_X with NH_3 at low temperature, Chem. Eng. J. 317 (2017) 20–31.

[14] S. Cai, H. Hu, H. Li, L. Shi, D. Zhang, Design of multi-shell Fe_2O_3@MnO_X@CNTs for the selective catalytic reduction of NO with NH_3: Improvement of catalytic activity and SO_2 tolerance, Nanoscale 8 (2016) 3588–3598.

[15] Z. Ma, H. Yang, F. Liu, X. Zhang, Interaction between SO_2 and Fe-Cu-O_X/CNTs-TiO_2 catalyst and its influence on NO reduction with NH_3, Appl. Catal., A 467 (2013) 450–455.

[16] P.S. Hammershøi, P.N.R. Vennestrøm, H. Falsig, A.D. Jensen, T.V.W. Janssens, Importance of the Cu oxidation state for the SO_2-poisoning of a Cu-SAPO-34 catalyst in the NH_3-SCR reaction, Appl. Catal., B 236 (2018) 377–383.

[17] H. Wang, Z. Qu, S. Dong, C. Tang, Mechanistic investigation into the effect of sulfuration on the FeW catalysts for the selective catalytic reduction of NO_X with NH_3, ACS Appl. Mater. Interfaces 9 (2017) 7017–7028.

[18] X. Li, C. Zhang, X. Zhang, W. Li, P. Tan, L. Ma, Q. Fang, G. Chen, Study on im-proving the SO_2 tolerance of low-temperature SCR catalysts using zeolite mem-branes: NO/SO_2 separation performance of aluminogermanate membranes, Chem. Eng. J. 335 (2018) 483–490.

[19] L. Ma, J. Li, R. Ke, L. Fu, Catalytic performance, characterization, and mechanism study of $Fe_2(SO_4)_3$/TiO_2 catalyst for selective catalytic reduction of NO_X by am-monia, J. Phys. Chem. C 115 (2011) 7603–7612.

[20] Y. Yu, J. Miao, J. Wang, C. He, J. Chen, Facile synthesis of $CuSO_4$/TiO_2 catalysts with superior activity and SO_2 tolerance for NH_3-SCR: Physicochemical properties and reaction mechanism, Catal. Sci. Technol. 7 (2017) 1590–1601.

[21] P.G.W.A. Kompio, A. Brückner, F. Hipler, O. Manoylova, G. Auer, G. Mestl, W. Grünert, V_2O_5-WO_3/TiO_2 catalysts under thermal stress: Responses of structure and catalytic behavior in the selective catalytic reduction of NO by NH_3, Appl. Catal., B 217 (2017) 365–377.

[22] M. Casanova, K. Schermanz, J. Llorca, A. Trovarelli, Improved high temperature stability of NH_3-SCR catalysts based on rare earth vanadates supported on TiO_2-WO_3-SiO_2, Catal. Today 184 (2012) 227–236.

[23] C.U.I. Odenbrand, Thermal stability of vanadia SCR catalysts for the use in diesel applications, Chem. Eng. Res. Des. 86 (2008) 663–672.

[24] A. Shi, X. Wang, T. Yu, M. Shen, The effect of zirconia additive on the activity and structure stability of V_2O_5/WO_3-TiO_2 ammonia SCR catalysts, Appl. Catal., B 106 (2011) 359–369.

[25] H. Tagawa, Thermal decomposition temperatures of metal sulfates, Thermochim. Acta 80 (1984) 23–33.

[26] L. Zhang, W. Zou, K. Ma, Y. Cao, Y. Xiong, S. Wu, C. Tang, F. Gao, L. Dong, Sulfated temperature effects on the catalytic activity of CeO_2 in NH_3-selective catalytic re-duction conditions, J. Phys. Chem. C 119 (2015) 1155–1163.

[27] S. Yang, Y. Guo, H. Chang, L. Ma, Y. Peng, Z. Qu, N. Yan, C. Wang, J. Li, Novel effect of SO_2 on the SCR reaction over CeO_2: Mechanism and significance, Appl. Catal., B 136–137 (2013) 19–28.

[28] L. Ma, C.Y. Seo, M. Nahata, X. Chen, J. Li, J.W. Schwank, Shape dependence and sulfate promotion of CeO_2 for selective catalytic reduction of NO_X with NH_3, Appl. Catal., B 232 (2018) 246–259.

[29] F. Liu, K. Asakura, H. He, W. Shan, X. Shi, C. Zhang, Influence of sulfation on iron titanate catalyst for the selective catalytic reduction of NO_X with NH_3, Appl. Catal., B 103 (2011) 369–377.

[30] Y. Peng, J. Li, W. Shi, J. Xu, J. Hao, Design strategies for development of SCR catalyst: Improvement of alkali poisoning resistance and novel regeneration method, Environ. Sci. Technol. 46 (2012) 12623–12629.

[31] M. Calatayud, C. Minot, Effect of alkali doping on a V_2O_5/TiO_2 catalyst from per-iodic DFT calculations, J. Phys. Chem. C 111 (2007) 6411–6417.

[32] Y. Yu, J. Miao, C. He, J. Chen, C. Li, M. Douthwaite, The remarkable promotional effect of SO_2 on Pb-poisoned V_2O_5-WO_3/TiO_2 catalysts: An in-depth experimental and theoretical study, Chem. Eng. J. 338 (2018) 191–201.

[33] C. He, Z. Jiang, M. Ma, X. Zhang, M. Douthwaite, J. Shi, Z. Hao, Understanding the promotional effect of Mn_2O_3 on micro-/mesoporous hybrid silica nanocubic-sup-ported Pt catalysts for the low-temperature destruction of methyl ethyl ketone: An experimental and theoretical Study, ACS Catal. 8 (2018) 4213–4229.

[34] M. Zhu, J.K. Lai, I.E. Wachs, Formation of N_2O greenhouse gas during SCR of NO with NH_3 by supported vanadium oxide catalysts, Appl. Catal., B 224 (2018) 836–840.

[35] H. Fu, X. Wang, H. Wu, Y. Yin, J. Chen, Heterogeneous uptake and oxidation of SO_2 on iron oxides, J. Phys. Chem. C 111 (2007) 6077–6085.

[36] Y. Yu, X. Meng, J. Chen, J. Wang, Y. Chen, New insight into the effect of potassium on commercial SCR Catalyst: Promotion of thermal stability, Water Air Soil Pollut. 226 (2015) 410.

[37] X. Zhang, Y. Yang, L. Song, Y. Wang, C. He, Z. Wang, L. Cui, High and stable cat-alytic activity of Ag/Fe_2O_3 catalysts derived from MOFs for CO oxidation, Mol. Catal. 447 (2018) 80–89.

[38] B.M. Reddy, I. Ganesh, E.P. Reddy, Study of dispersion and thermal stability of V_2O_5/TiO_2-SiO_2 catalysts by XPS and other techniques, J. Phys. Chem. B 101 (1997) 1769–1774.

[39] X. Zhang, H. Li, X. Lv, J. Xu, Y. Wang, C. He, N. Liu, Y. Yang, Y. Wang, Facile synthesis of highly efficient amorphous Mn-MIL-100 catalysts: Formation me-chanism and structure changes during application in CO oxidation, Chem. Eur. J. 24 (2018) 8822–8832.

[40] M. Tian, Y. Jian, M. Ma, C. He, C. Chen, C. Liu, J. Shi, Rational design of CrO_X/$LaSrMnCoO_6$ composite catalysts with superior chlorine tolerance and stability for 1,2-dichloroethane deep destruction, Appl. Catal., A 570 (2019) 62–72.

[41] X. Du, X. Gao, L. Cui, Y. Fu, Z. Luo, K. Cen, Investigation of the effect of Cu addition on the SO_2-resistance of a CeTi oxide catalyst for selective catalytic reduction of NO with NH_3, Fuel 92 (2012) 49–55.

[42] Y. He, M.E. Ford, M. Zhu, Q. Liu, U. Tumuluri, Z. Wu, I.E. Wachs, Influence of catalyst synthesis method on selective catalytic reduction (SCR) of NO by NH_3 with V_2O_5-WO_3/TiO_2 catalysts, Appl. Catal., B 193 (2016) 141–150.

[43] H. Huang, Y. Lan, W. Shan, F. Qi, S. Xiong, Y. Liao, Y. Fu, S. Yang, Effect of sulfation on the selective catalytic reduction of NO with NH_3 over γ-Fe_2O_3, Catal. Lett. 144 (2014) 1–7.

[44] H. Chen, Y. Xia, H. Huang, Y. Gan, X. Tao, C. Liang, J. Luo, R. Fang, J. Zhang, W. Zhang, X. Liu, Highly dispersed surface active species of Mn/Ce/TiW catalysts for high performance at low temperature NH_3-SCR, Chem. Eng. J. 330 (2017) 1195–1202.

[45] R. Guo, X. Sun, J. Liu, W. Pan, M. Li, S. Liu, P. Sun, S. Liu, Enhancement of the NH_3-SCR catalytic activity of $MnTiO_X$ catalyst by the introduction of Sb, Appl. Catal., A 558 (2018) 1–8.

[46] A. Marberger, D. Ferri, M. Elsener, O. Kröcher, The significance of Lewis acid sites for the selective catalytic reduction of nitric oxide on vanadium-based catalysts, Angew. Chem. Int. Ed. 55 (2016) 11989–11994.

[47] M. Kong, Q. Liu, J. Zhou, L. Jiang, Y. Tiian, J. Yang, S. Ren, J. Li, Effect of different

potassium species on the deactivation of V_2O_5-WO_3/TiO_2 SCR catalyst: Comparison of K_2SO_4, KCl and K_2O, Chem. Eng. J. 348 (2018) 637–643.
[48] M. Salazar, S. Hoffmann, V. Singer, R. Becker, W. Grünert, Hybrid catalysts for the selective catalytic reduction (SCR) of NO by NH_3. On the role of fast SCR in the reaction network, Appl. Catal., B 199 (2016) 433–438.
[49] Y. Yu, J. Chen, J. Wang, Y. Chen, Performances of $CuSO_4$/TiO_2 catalysts in selective catalytic reduction of NO_x by NH_3, Chin. J. Catal. 37 (2016) 281–287.
[50] Z. Jiang, C. He, N.F. Dummer, J. Shi, M. Tian, C. Ma, Z. Hao, S.H. Taylor, M. Ma, Z. Shen, Insight into the efficient oxidation of methyl-ethyl-ketone over hier-archically micro-mesostructured Pt/K-(Al)SiO_2 nanorod catalysts: Structure-activity relationships and mechanism, Appl. Catal., B 226 (2018) 220–233.
[51] J.G. Amores, V.S. Escribano, G. Ramis, G. Busca, An FT-IR study of ammonia adsorption and oxidation over anatase-supported metal oxides, Appl. Catal., B 13 (1997) 45–58.
[52] Y. Yu, J. Wang, J. Chen, X. Meng, Y. Chen, C. He, Promotive effect of SO_2 on the activity of a deactivated commercial selective catalytic reduction catalyst: An in situ DRIFT Study, Ind. Eng. Chem. Res. 53 (2014) 16229–16234.
[53] H. Zhang, Y. Zou, Y. Peng, Influence of sulfation on CeO_2-ZrO_2 catalysts for NO reduction with NH_3, Chin. J. Catal. 38 (2017) 160–167.
[54] T.S. Kurtikyan, P.C. Ford, FTIR and optical spectroscopic studies of the reactions of heme models with nitric oxide and other NO_x in porous layered solids, Coord. Chem. Rev. 252 (2008) 1486–1496.
[55] D. Meng, W. Zhan, Y. Guo, Y. Guo, L. Wang, G. Lu, A highly effective catalyst of Sm-MnO_x for the NH_3-SCR of NO_x at low temperature: Promotional role of Sm and its catalytic performance, ACS Catal. 5 (2015) 5973–5983.
[56] L. Wei, S. Cui, H. Guo, X. Ma, L. Zhang, DRIFT and DFT study of cerium addition on SO_2 of manganese-based catalysts for low temperature SCR, J. Mol. Catal., A 421 (2016) 102–108.
[57] X. Guo, C. Bartholomew, W. Hecker, L.L. Baxter, Effects of sulfate species on V_2O_5/TiO_2 SCR catalysts in coal and biomass-fired systems, Appl. Catal., B 92 (2009) 30–40.
[58] F. Cao, S. Su, J. Xiang, L. Sun, S. Hu, Q. Zhao, P. Wang, S. Lei, Density functional study of adsorption properties of NO and NH_3 over CuO/γ-Al_2O_3 catalyst, Appl. Surface Sci. 261 (2012) 659–664.
[59] Y. Peng, W. Si, X. Li, J. Luo, J. Li, J. Crittenden, J. Hao, Comparison of MoO_3 and WO_3 on arsenic poisoning V_2O_5/TiO_2 catalyst: DRIFTS and DFT study, Appl. Catal., B 181 (2016) 692–698.